Two distinct immunopathological profiles in lungs of lethal COVID-19

Short title: Profiles of COVID-19 lungs

Ronny Nienhold[1§], Yari Ciani[2§], Viktor H. Koelzer[3,4§], Alexandar Tzankov[5], Jasmin D. Haslbauer[5], Thomas Menter[5], Nathalie Schwab[1], Maurice Henkel[1], Angela Frank[1], Veronika Zsikla[1], Niels Willi[1], Werner Kempf[6], Thomas Hoyler[7], Mattia Barbareschi[8], Holger Moch[3], Markus Tolnay[5], Gieri Cathomas[1], Francesca Demichelis[2,9]*, Tobias Junt[7]*, Kirsten D. Mertz[1]*

Affiliations:

[1] Institute of Pathology, Cantonal Hospital Baselland, Liestal, Switzerland

[2] Laboratory of Computational and Functional Oncology, Department for Cellular, Computational and Integrative Biology – CIBIO, University of Trento, Trento, Italy

[3] Department of Pathology and Molecular Pathology, University Hospital Zurich, Zurich, Switzerland

[4] Department of Oncology and Nuffield Department of Medicine, University of Oxford, Oxford, United Kingdom

[5] Pathology, Institute of Medical Genetics and Pathology, University Hospital Basel, Basel, Switzerland

[6] Kempf und Pfaltz Histologische Diagnostik, Zurich, Switzerland

[7] Novartis Institutes for BioMedical Research (NIBR), Basel, Switzerland

[8] Anatomia ed Istologia Patologica, Ospedale S. Chiara di Trento, Trento, Italy

[9] Caryl and Israel Englander Institute for Precision Medicine, Institute for Computational Biomedicine, New York Presbyterian Hospital, Weill Cornell Medicine, New York, New York, USA

[§] These authors jointly contributed to this work.

* These authors jointly directed this work.

Word count: Abstract 87 / Main text 1889

Correspondence:

PD Dr. med. Kirsten D. Mertz, MD PhD

Institute of Pathology Liestal

Cantonal Hospital Baselland

Mühlemattstrasse 11

CH-4410 Liestal, Switzerland

Phone: + 41 (0) 61 925 2635

Email: kirsten.mertz@ksbl.ch

Abstract

Immune responses in lungs of Coronavirus Disease 2019 (COVID-19) are poorly characterized. We conducted transcriptomic, histologic and cellular profiling of *post mortem* COVID-19 and normal lung tissues. Two distinct immunopathological reaction patterns were identified. One pattern showed high expression of interferon stimulated genes (ISGs) and cytokines, high viral loads and limited pulmonary damage, the other pattern showed severely damaged lungs, low ISGs, low viral loads and abundant immune infiltrates. Distinct patterns of pulmonary COVID-19 immune responses correlated to hospitalization time and may guide treatment and vaccination approaches.

COVID-19 is a pandemic respiratory disease with 2-3% lethality[1]. While a coronavirus (SARS-CoV-2) is the causative agent, the antiviral immune response- may also contribute to devastating end organ damage[2]. Therefore analysis of *post mortem* tissues is critical for the mechanistic understanding of COVID-19 pathophysiology[3].

Here we analyzed 34 *post mortem* lung samples from 16 deceased COVID-19 patients and 9 *post mortem* lung samples from 6 patients who died from non-infectious causes (**Extended Data Table 1**). Of note, we did not find bacterial superinfections in COVID-19 lungs except in three samples (**Extended Data Figure 1**). Differential gene expression analysis based on a commercial assay (OIRRA) designed for quantification of immune cell and inflammatory transcripts (**Extended Data Table 2**) identified 68 up-regulated and 30 down-regulated genes in COVID-19 infected lungs compared to normal tissue (**Extended Data Table 3**). Using a consensus of 30 different indices[4] we identified by K-means clustering three groups of samples defined by the expression levels of the deregulated genes (**Figure 1a, Extended Data Figure 2**). Clusters 1 (50% of samples) and 2 (41%) contained COVID-19 samples and cluster 3 contained all normal lung samples and 3 COVID-19 samples (9%). To understand why the majority of COVID-19 lung tissues segregated into defined clusters 1 or 2, we undertook a gene ontology analysis. We identified interferon stimulated genes (ISGs) as a key upregulated pathway in COVID-19 autopsy lungs (**Figure 1b**), which was differentially represented in cluster 1 and 2, respectively (**Figure 1c**). Identification of an ISG high cluster (Cluster 1, ISG^{high}) was surprising, since SARS-CoV-2 was proposed to lead to limited ISG induction, yet only in comparison to other respiratory viruses[5]. Next, we analyzed frequencies of specific immune cells in lungs by computational image analysis. T cells (CD3+), particularly CD8+ T cells, and macrophages (CD68+, CD163+) were selectively enriched in samples from the ISG^{low} cluster 2 (**Figure 1d**), as were CD4+ T cells, while CD20+ B cells and CD123+ plasmacytoid dendritic cells (pDCs) did not show differential frequencies between ISG^{high} and ISG^{low} lungs (**Extended Data Figure 3a**,**b**). Since T cell exhaustion was observed in COVID-19[6], we compared frequencies of CD8+PD1+ cells in ISG^{high} and

ISG^{low} samples, and observed a higher frequency of CD8+PD1+ T-cells in the ISG^{low} subgroup, potentially indicative of advanced disease (**Extended Data Figure 3a**,**b**). Histological analysis of COVID-19 lung tissues revealed striking pulmonary damage exclusively in ISG^{low} samples, with distinct peri-alveolar foci of infiltrating CD68+ macrophages and CD8+ T cells (**Figure 1e**).

Expression of ISGs was tightly correlated with pulmonary viral load (**Figure 2a**), and immunohistochemical staining showed SARS-CoV-2 nucleocapsid protein mostly in pneumocytes of ISG^{high} lungs (**Figure 2b**). Since a cytokine storm has been proposed to cause adverse outcome of COVID-19[7], and cytokines were highly expressed in bronchoalveolar lavages (BALs) of COVID-19 patients[8], we investigated expression of a pro-inflammatory cytokine signature (TNF, IL6, IL1b, CCL2, IFNA17, IFNB1, CXCL9, CXCL10, CXCL11) in lung samples from lethal COVID-19. The proinflammatory gene signature was significantly enriched in the ISG^{high} subset (**Figure 2c**), but was not associated with alveolar hemorrhage (**Figure 2d**). Within this cytokine signature, co-regulated subgroups (IL1B/IL6/TNF, IFNB1/IFNA17, CCL2/CXCL9/CXCL19/CXCL11) were identified (**Figure 2e**). Importantly, only the CXCL9/10/11 sub-signature was positively associated with alveolar hemorrhage (**Figure 2f, Extended Data Figure 4**). This is in line with observations that these chemokines compromise endothelial integrity via CXCR3[9], and that CXCL10 is a key determinant of severe COVID-19[10]. Interestingly, basal levels of CXCL9 or CXCL10 are elevated in elderly, hypertensive and obese individuals, which were strongly represented in our autopsy cohort and are predisposed to severe COVID-19[11,12]. Of note, our study could not take extrapulmonary cytokine sources or effects into account.

Since none of the above pulmonary cytokine sub-signatures was positively associated with diffuse alveolar damage (DAD, **Extended Data Figure 5**), we investigated which other local immune signature showed this association. We found a strong association of DAD with low expression of ISGs (**Figure 2g**), and an activated CD8+ T cell signature (CD38, GZMA, GZMB, CCR5, **Figure 2h**), yet not with pulmonary CD8+ T-cell infiltration (**Figure 2i**). In addition, the activated CD8+ signature was inversely correlated to viral counts, particularly in ISG^{low} cases (**Figure 2j**). Therefore we speculate that activated CD8+ T cells are essential for virus elimination, similar to murine models of coronavirus infection[13], yet it is possible that they contribute to pulmonary damage as well. Of note, ISG^{low} samples also expressed elevated p53 and Ki67 (**Figure 2k**), i.e. reactive markers of DAD which indicate lung remodeling[14]. Since the ISG^{low} pattern showed lower viral counts, higher accumulation and activation of CD8+ T cells in tissues and accrual of pulmonary damage and remodeling, the ISG^{low} phase may follow an earlier ISG^{high} phase during the course of infection. This was supported by significantly longer hospitalization in COVID-19 patients from whom ISG^{low} lung samples were obtained (**Figure 2l**). This is in line with epidemiologic data showing that one defined group of critical COVID-19 patients quickly succumbs to disease after hospitalization, while others die after longer intensive care[15].

Discovery of two patterns of immunopathology in COVID19 *post mortem* lungs suggests that only patients with an ISG^{high} pattern show high viral loads and may benefit from antivirals. ISG^{low} patients

instead show low viral loads yet strong complement activation in lungs (**Figure 2m**) and thus may potentially benefit from complement inhibition[16]. In addition, the ISG^{low} pattern suggests that CD8+ T cells are involved in antiviral protection and should be considered for vaccination efforts.

References

1. Hopkins, J. Corona virus resource center. Latest update: 05/22/2020: https://coronavirus. jhu. edu/data (2020).
2. Chen, G., et al. Clinical and immunological features of severe and moderate coronavirus disease 2019. The Journal of clinical investigation 130(2020).
3. Menter, T., et al. Post-mortem examination of COVID19 patients reveals diffuse alveolar damage with severe capillary congestion and variegated findings of lungs and other organs suggesting vascular dysfunction. Histopathology (2020).
4. Charrad, M., Ghazzali, N., Boiteau, V. & Niknafs, A. NbClust Package: finding the relevant number of clusters in a dataset. J. Stat. Softw (2012).
5. Blanco-Melo, D., et al. Imbalanced host response to SARS-CoV-2 drives development of COVID-19. Cell (2020).
6. Diao, B., et al. Reduction and functional exhaustion of T cells in patients with coronavirus disease 2019 (COVID-19). Frontiers in Immunology 11, 827 (2020).
7. Huang, C., et al. Clinical features of patients infected with 2019 novel coronavirus in Wuhan, China. The lancet 395, 497-506 (2020).
8. Liao, M., et al. Single-cell landscape of bronchoalveolar immune cells in patients with COVID-19. Nature Medicine, 1-3 (2020).
9. Bodnar, R.J., Yates, C.C., Rodgers, M.E., Du, X. & Wells, A. IP-10 induces dissociation of newly formed blood vessels. Journal of cell science 122, 2064-2077 (2009).
10. Yang, Y., et al. Exuberant elevation of IP-10. MCP-3 and IL-1ra during SARS-CoV-2 infection is associated with disease severity and fatal outcome. medRxiv 2002, 2020 (2020).
11. Hueso, L., et al. Upregulation of angiostatic chemokines IP-10/CXCL10 and I-TAC/CXCL11 in human obesity and their implication for adipose tissue angiogenesis. Int J Obes (Lond) 42, 1406-1417 (2018).
12. Bonfante, H.L., et al. CCL2, CXCL8, CXCL9 and CXCL10 serum levels increase with age but are not altered by treatment with hydroxychloroquine in patients with osteoarthritis of the knees. Int J Rheum Dis 20, 1958-1964 (2017).
13. Cupovic, J., et al. Central Nervous System Stromal Cells Control Local CD8(+) T Cell Responses during Virus-Induced Neuroinflammation. Immunity 44, 622-633 (2016).
14. Shetty, S.K., et al. p53 and miR-34a Feedback Promotes Lung Epithelial Injury and Pulmonary Fibrosis. Am J Pathol 187, 1016-1034 (2017).
15. Salje, H., et al. Estimating the burden of SARS-CoV-2 in France. Science (2020).
16. Magro, C., et al. Complement associated microvascular injury and thrombosis in the pathogenesis of severe COVID-19 infection: a report of five cases. Transl Res (2020).

Methods

Ethics statement

This study was conducted according to the principles expressed in the Declaration of Helsinki. Ethics approval was obtained from the Ethics Committee of Northwestern and Central Switzerland (Project-ID 2020-00629). For all patients, either personal and/or family consent was obtained for autopsy and sample collection.

Patients and sample collection

The study is based on the analysis of 16 out of 21 consecutive COVID-19 autopsies performed between March 9th and April 14th 2020 at the Institute of Pathology Liestal and Institute of Medical Genetics and Pathology Basel, Switzerland. Clinical features including symptoms, course of disease, comorbidities, laboratory results and therapy are listed in **Extended Data Table 1a**. Detailed autopsy findings for each patient were recently published, and the identifiers (with the prefix "C") for each COVID-19 patient are consistent with the description of this Swiss COVID-19 autopsy cohort[3]. In this study, we analysed formalin fixed and paraffin embedded (FFPE) lung tissue of distinct areas of the lungs of 16 of these COVID-19 patients. All 16 COVID-19 patients had positive nasopharyngeal swabs collected while alive. In all COVID-19 patients, diagnosis was confirmed by detection of SARS-CoV-2 in postmortal lung tissues. 5/16 patients were additionally tested by postmortal nasopharyngeal swabs which were positive for SARS-CoV-2 in all 5 cases.

As a control cohort, we selected 6 autopsies performed between January 2019 and March 2020 at the Institute of Pathology Liestal ("normal" patients N1 – N6). These control patients died of other, non-infectious causes and had a similar age, gender and cardiovascular risk profile. Patients with infections were excluded from this control cohort. Another control cohort consisted of 4 autopsies of patients suffering from various infections mainly with bacteria affecting the lung (patients with lung pathology, P1 – P4). Details for both control cohorts are listed in **Extended Data Table 1b**,**c**. SARS-CoV-2 was ruled out for each control patient by PCR-examination of lung tissue samples.

Nucleic acid extraction

RNA was extracted from up to six sections of FFPE tissue blocks using RecoverAll Total Nucleic Acid Isolation Kit (Cat No. AM1975, Thermo Fisher Scientific, Waltham, MA, USA). Extraction of DNA from up to 10 sections of FFPE tissue samples was automated by EZ1 Advanced XL (Qiagen, Hilden,

Germany) using the EZ1 DNA Tissue Kit (Cat No. 953034, Qiagen, Hilden, Germany). Concentration of DNA and RNA were measured with Qubit 2.0 Fluorometer and Qubit dsDNA HS Assay or Qubit RNA HS Assay (Cat No. Q33230 & Q32852, Thermo Fisher Scientific, Waltham, MA, USA), respectively.

Quantification of SARS-CoV-2 in FFPE tissue samples

Post mortem viral load was individually measured in all lung tissue blocks from all patients included in this study. SARS-CoV-2 was detected in 15ng of human total RNA using the TaqMan 2019-nCoV Assay Kit v1 (Cat No. A47532, Thermo Fisher Scientific, Waltham, MA, USA), which targets three genomic regions (ORFab1, S Protein, N Protein) specific for SARS-CoV-2 and the human RNase P gene (RPPH1). The copy numbers of the SARS-CoV-2 viral genome was determined by utilizing the TaqMan 2019-nCoV Control Kit v1 (Cat No. A47533, Thermo Fisher Scientific, Waltham, MA, USA) and a comparative "ΔΔCт" method. The control kit contains a synthetic sample with a defined amount of target molecules for the human RPPH1 and the three SARS-CoV-2 assays, and was re-analyzed in parallel with patient samples. For each patient sample, this method resulted in individual copy numbers of the human RPPH1 and the three SARS-CoV-2 targets. Finally, the mean copy number of the SARS-CoV-2 targets was normalized to 1 x 10^6 RPPH1 transcripts.

Profiling of immune response by targeted RNAseq

The expression levels of 398 genes, including genes relevant in innate and adaptive immune response and housekeeping genes for normalization, were analyzed with the Oncomine Immune Response Research Assay (OIRRA, Cat No. A32881, Thermo Fisher Scientific, Waltham, MA, USA). The OIRRA is a targeted gene expression assay designed for the Ion™ next-generation sequencing (NGS) platform. This gene expression assay was originally designed to interrogate the tumor microenvironment to enable mechanistic studies and identification of predictive biomarkers for immunotherapy in cancer. The assay is optimized to measure the expression of genes involved in immune cell interactions and signaling, including genes expressed at low levels and involved in inflammatory signaling. The 398 genes covered by this assay are listed in **Extended Data Table 2**.

The NGS libraries were prepared as recommended by the supplier. In brief, 30ng of total RNA were used for reverse transcription (SuperScript VILO, Cat No. 11754250, Thermo Fisher Scientific, Waltham, MA, USA) and subsequent library preparation. The libraries were quantified (Ion Library TaqMan Quantitation Kit, Cat No. 4468802, Thermo Fisher Scientific, Waltham, MA, USA), equimolarly pooled and sequenced utilizing the Ion GeneStudio S5xl (Thermo Fisher Scientific,

Waltham, MA, USA). De-multiplexing and gene expression level quantification were performed with the standard setting of the ImmuneResponseRNA plugin (version 5.12.0.1) within the Torrent Suite (version 5.12.1), provided as part of the OIRRA by Thermo Fisher Scientific, Waltham, MA, USA.

Detection of co-infections by whole genome sequencing

To identify potential pathogens accompanying an infection with SARS-CoV-2, we analyzed the DNA of the same tissue samples used for detection and profiling of the SARS-CoV-2-specific immune response. First, 250ng of genomic DNA was enzymatically sheared (15 minutes at 37°C) and barcoded using the Ion Xpress Plus Fragment Library Kit (Cat No. 4471269, Thermo Fisher Scientific, Waltham, MA, USA). Subsequently, the libraries were quantified (Ion Library TaqMan Quantitation Kit, Cat No. 4468802, Thermo Fisher Scientific, Waltham, MA, USA) and up to three libraries were pooled at equimolar levels for analysis with Ion GeneStudio S5xl (Thermo Fisher Scientific, Waltham, MA, USA). Sequencing data for each sample was analysed using the CLC genomics workbench (version 20.0.3, Qiagen, Hilden, Germany) in combination with the microbial genomics module (version 20.0.1, Qiagen, Hilden, Germany): The raw reads were trimmed by quality (Mott algorithm with limit 0.05 and a maximum of 2 ambiguous bases per read) and mapped to the human genome (GRCh37 hg19, match score: 1, mismatch cost: 2, indel opening cost: 6, indel extension cost: 1). Unmapped reads were analysed by taxonomic profiling to identify reads of viral or bacterial origin. The profiling utilized an index of 11’540 viral genomes with a minimum length of 1’000 bp and 2’715 bacterial reference genomes with a minimum length of 500’000 bp, retrieved from the NCBI Reference Sequence Database (date of download: 2020-04-02).

Immunohistochemistry

Immunohistochemical analyses for CD3, CD4, CD8, CD15, CD20, CD68, CD123, CD163, PD-1, MPO, p53, Ki67, C3d and C5b-9 were performed on all lung tissue blocks used in this study. Antibodies, staining protocols and conditions are detailed in **Extended Data Table 4**.

Qualitative and semiquantitative assessment of histopathological lung damage and neutrophilic infiltration

Hematoxylin and eosin (H&E) and Elastica van Gieson (EvG) stained sections of all lung tissues used in this study were independently evaluated by two experienced and board certified pathologists (VZ and KDM) (**Extended Data Table 5**). Both pathologists evaluated the presence of diffuse alveolar damage (DAD), and if present, its stage, intra-alveolar edema and hemorrhage. In addition, both

pathologists evaluated the severity of histopathological changes in COVID-19 lungs (1 = mild / discrete alterations, 2 = moderate, 3 = severe changes) based on resemblance between normal and pathologically altered lung tissues. Parameters that were taken into account included reduction of alveolar air-filled spaces, typical histologic features of DAD with hyaline membrane formation, infiltration of lymphocytes, monocytes and neutrophils into interstitial and alveolar spaces, type 2 pneumocyte hyperplasia, desquamation of pneumocytes, histologic features of organizing pneumonia including intra-alveolar fibrin deposition and fibrosis (acute fibrinous and organizing pneumonia, AFOP)[17,18]. The number of neutrophils per lung tissue section was estimated on H&E stained sections and by immunohistochemical stains for CD15 and MPO using a three tiered system (1 = few or no neutrophils, 2 = moderate number of neutrophils, 3 = high number of neutrophils). Assessment of the two pathologists was concordant in the vast majority of cases. Discrepant cases were reviewed by a third pathologist (NW) to reach consent.

Digital image analysis

Slides were digitalized on a 3DHistech™ P1000 slide scanner at 400x magnification (3DHISTECH Ltd. Budapest, Hungary). Digital slide review and quality control was performed by a board-certified pathologist (VHK). Tissue regions with staining artefacts, folds or other technical artefacts were excluded from analysis. A deep neural network (DNN) algorithm (Simoyan and Zisserman VGG, HALO AI™ on HALO™ 3.0.311.167, Indica Labs, Corrales, NM) was trained using pathologist annotations to automatically localize and measure the area of each lung tissue sample on the digital slides. Background regions and glass were excluded from analysis. Mark-up images for tissue classification were generated and classification accuracy was confirmed through pathology review. For cell-level analysis, color deconvolution for DAB, AP and hematoxylin channels was performed and nuclear segmentation was optimized using cell-morphometric parameters. Marker-positive cells in stromal and epithelial regions were quantified. For CD3, CD4, CD8, CD20, CD68, CD123, CD163 and PD1, staining detection was optimized for the cytoplasmic / membranous compartment and marker expression was measured on a continuous scale at single cell resolution. For assessment of CD8/PD1 double stains, color deconvolution was optimized for separation of DAB (PD1) and AP (CD8) staining products. Internal controls (non-immune cells) and external controls (tonsil) were used to calibrate the detection limits and cross-validated by visual review. For each tissue sample, the total area of lung tissue in mm^2, the absolute number of marker-positive cells, cell morphometric parameters and staining intensity were recorded.

Identification of SARS-CoV-2 immune response pattern

Gene expression analysis

Samples were included in the study based on quality of libraries and alignment performance. Applied inclusion criteria are: >1 million of mapped reads, good concentration of libraries, average read length >100bp, > 300 target genes with more than 10 reads. One sample with > 1 Mio reads was excluded from the study because of shorter read length and a low library concentration. Notably this sample had the longest time between death and autopsy (72h) before analysis. Differential expression analysis was performed using the edgeR package comparing normal lung samples, COVID-19 samples and samples from patients with other infections. Genes were selected for downstream analyses by fdr <0.05 and |logFC| >1 for clustering analysis. Clustering analysis was performed using k-means algorithm and complete linkage. Ideal number of clusters (n=3) was chosen based on 30 different algorithms[19] and the final clustering derives from the consensus of 2000 iterations. Expression of gene signatures was calculated as median of log2(cpm + 1) of selected genes.

Functional enrichment analysis

Biological processes enrichment was performed using the enrichGO function of the package clusterProfiler[20] setting all the genes included in the assay as universe.

Statistical analysis

All the analyses and graphical representations were performed using the R statistical environment software[21] and the following packages: ggplot2[22], circlize[23], ComplexHeatmap[24], ggfortify[25], reshape2[26] and factoextra[27]. Correlation between transcripts and viral counts was performed using Pearson's correlation. Association between continuous and categorical data were tested using Wilcoxon rank sum test.

Box-plots elements indicate the median (center line), upper and lower quartiles (box limits) and show all the data points. Whiskers extend to the most extreme value included in 1.5x interquartile range.

Figure Legends

Figure 1. Transcriptomic and immunologic profile of COVID-19 autopsy lungs.

(**a**) Heatmap showing K-means clustering of COVID-19 and normal lung samples based on expression levels of deregulated genes in COVID-19 versus normal lungs. (**b**) Gene ontology enrichment analysis of genes upregulated in COVID-19 samples. (**c**) ISG signature expression in clusters 1 and 2 of COVID-19 lungs. (**d**) Frequencies of immune cells on ISG^{high} and ISG^{low} COVID-19 lung sections and controls. (**e**) Representative H&E stains and immunohistochemistry (CD3, CD8, CD68, CD163) of ISG^{high} and ISG^{low} COVID-19 lungs and controls, size bar 500 µm.

Figure 2. Relationship between cytokine signature and histopathological changes.

(**a**) Correlation of viral load and ISG expression in COVID-19 lungs. Solid lines, sample data from the same patient. Dotted line, regression for all samples and 95% CI (Pearson's correlation=0.83, adjusted R-squared=0.68, p-value=1.66e-08). (**b**) Representative immunohistochemistry for SARS-CoV-2 on ISG^{high} and ISG^{low} COVID-19 lung samples and controls. Size bar 100 µm. (**c**) Expression of a cytokine signature (IL-1b, IL6, TNF, IFNa17, IFNb1, CCL2, CXCL9, CXCL10, CXCL11) in ISG^{high} and ISG^{low} COVID-19 lung samples. (**d**) Association of the cytokine signature with intraalveolar hemorrhage. (**e**) Pearson's correlation of pro-inflammatory cytokines in the cytokine signature indicates presence of co-regulated cytokines. (**f**) Association of CXCL9/10/11 expression in lung samples with intraalveolar hemorrhage. Association of DAD stage with (**g**) ISG expression, (**h**) activated CD8+ T cell signature, (**i**) CD8 T cell counts. (**j**) Inverse correlation of viral load and activated CD8+ T cell signature. Solid line, sample data from the same patient. Dotted line, regression for all the samples and 95% CI (Pearson's correlation=-0.5 adjusted R-squared=0.22, p-value=0.005). (**k**) Representative immunohistochemistry for p53 and Ki67. Size bar 100 µm. (**l**) Hospitalization time in ISG^{low} patients versus ISG^{high} patients. (**m**) Representative IHC staining for complement activation products C5b-9 and C3d in ISG^{high}, ISG^{low} COVID-19 and normal control lungs. Size bar 100 µm. ISG^{high} samples, red; ISG^{low} samples, blue.

Extended Data Figure 1. Co-infections in COVID-19 lungs identified by WGS metagenomics.

(**a**) Total number of reads generated for each sample. (**b**) Percentage of reads and (**c**) absolute numbers of reads not mapping to the human genome (GRCh37 hg19). (**d**) Bacterial and (**e**) viral co-infections across lung samples, WGS metagenomic analysis. Purple dots, numbers of reads sufficient for identification of non-human species. Samples are ordered by increasing SARS-CoV-2 viral load in each group. Stacked bars, relative abundance of the most common species. Grey bars represent frequent species, colored bars show pathogenic species. *One COVID-19 patient (C3) clustered in the normal control group.

Extended Data Figure 2: Transcriptomics of COVID-19 and non-COVID-19 lung samples.
(**a**) Heatmap showing K-means clustering of COVID-19 and normal lung samples; version of Figure 1a with annotated gene names. (**b**) Comparison of up- and down-regulated genes in lung samples from COVID-19 patients, normal lung samples and other bacterial / viral pneumonia samples (**Extended Data Figure 1**). (**c**) Principal component analysis (PCA) of all lung samples reveals segregation based on diagnosis and viral load.

Extended Data Figure 3. Immune cell infiltrate on COVID-19 lung sections.
(**a**) Frequencies of immune cells on ISG^{high} and ISG^{low} COVID-19 lung sections and controls. (**b**) Representative immunohistochemistry (CD4, CD20, CD123, CD8/PD1) of ISG^{high} and ISG^{low} COVID-19 lungs and controls, size bar 500 µm.

Extended Data Figure 4. Association of cytokine signatures in ISG^{high} and ISG^{low} COVID-19 lung samples with intraalveolar hemorrhage.
Association of: (**a**) Median IL6, TNF, IL1B expression in ISG^{high} and ISG^{low} COVID-19 lung tissue with presence of intraalveolar hemorrhage. (**b**) Median IFNA17, IFNB1 expression in ISG^{high} and ISG^{low} COVID-19 lung tissue with presence of intraalveolar hemorrhage. (**c**) Median CCL2 expression in ISG^{high} and ISG^{low} COVID-19 lung tissue with presence of intraalveolar hemorrhage.

Extended Data Figure 5. Association of cytokine signatures in ISG^{high} and ISG^{low} COVID-19 lung samples with DAD stage.
Association of: (**a**) Median IL6, TNF, IL1B expression in ISG^{high} and ISG^{low} COVID-19 lung tissue with DAD stage. (**b**) Median IFNA17, IFNB1 expression in ISG^{high} and ISG^{low} COVID-19 lung tissue with DAD stage. (**c**) Median CXCL9/10/11 expression in ISG^{high} and ISG^{low} COVID-19 lung tissue with DAD stage. (**d**) Median CCL2 expression in ISG^{high} and ISG^{low} COVID-19 lung tissue with DAD stage.

Data availability

The datasets generated and analysed during this study can be accessed in GEO (GSE151764) and are available from the corresponding author upon request.

References

17. Copin, M.-C., Parmentier, E., Duburcq, T., Poissy, J. & Mathieu, D. Time to consider histologic pattern of lung injury to treat critically ill patients with COVID-19 infection. Intensive Care Medicine, 1-3 (2020).
18. Xu, Z., et al. Pathological findings of COVID-19 associated with acute respiratory distress syndrome. Lancet Respir Med 8, 420-422 (2020).
19. Bates, D., Mächler, M., Bolker, B. & Walker, S. Fitting linear mixed-effects models using lme4. arXiv preprint arXiv:1406.5823 (2014).
20. Chikina, M., Robinson, J.D. & Clark, N.L. Hundreds of genes experienced convergent shifts in selective pressure in marine mammals. Molecular biology and evolution 33, 2182-2192 (2016).
21. Team, R.C. R: A language and environment for statistical computing. (2013).
22. Wickham, H. ggplot2: elegant graphics for data analysis, (Springer, 2016).
23. Gu, Z., Gu, L., Eils, R., Schlesner, M. & Brors, B. circlize implements and enhances circular visualization in R. Bioinformatics 30, 2811-2812 (2014).
24. Gu, Z., Eils, R. & Schlesner, M. Complex heatmaps reveal patterns and correlations in multidimensional genomic data. Bioinformatics 32, 2847-2849 (2016).
25. Horikoshi, M. & Tang, Y. ggfortify: Data visualization tools for statistical analysis results. v0. 1.0. URL http://CRAN. R-project. org/package= ggfortify. R package version 0.4 1, 28 (2018).
26. Wickham, H. Reshaping data with the reshape package. Journal of statistical software 21, 1-20 (2007).
27. Kassambara, A. & Mundt, F. Package ‘factoextra’. Extract and visualize the results of multivariate data analyses 76(2017).

Acknowledgements

VHK gratefully acknowledges funding by the Promedica Foundation (F-87701-41-01). AT, JDH, TM and KDM are supported by and gratefully acknowledge the Botnar Research Centre for Child Health. We would like to thank Christian Tosch, Beat Béni, Daniel Turek, Melanie Sachs, Anne Graber, Christina Herz, Arbeneshe Berisha, Norbert Wey and the USZ pathology IT team, André Fitsche, Marcel Glönkler, Christiane Mittman and the USZ pathology laboratory team for expert technical support and scanning of slides.

Author contributions

RN, YC, VHK, FD, TJ and KDM jointly conceived the study, performed data interpretation and prepared the manuscript. AT, MB, HM, MT and CA provided intellectual input, provided critical resources and critically reviewed the manuscript. RN, YC, VHK, MH, TH and TJ performed bioinformatic and statistical analysis. AT, JDH, TM, NS, AF collected autopsy specimens and patient data. VZ, NW, WK and CA performed histomorphological evaluation. All authors approved the final manuscript.

Competing interests

VHK has served as an invited speaker on behalf of Indica Labs. TH and TJ are employees of Novartis. The other authors declare no competing interests.

Extended Data Table 1a. Clinical Data, COVID-19 cohort (16 patients)

Characteristics	N or x	% or range
Time between symptoms and death	7,4 d	0 - 20 d
Hospitalisation	5,6 d	0 - 13 d
Postmortem interval	28,4 h	11 - 67 h
Age	75 y	53 - 96 y
Sex	M 13 : F 3	
Comorbidities		
Hypertension	16	100 %
Cardiovascular disease	11	68 %
(Pre-)Adipositas	12	75 %
Diabetes	6	37,5 %
Initial clinical presentation		
Cough	13	81,25 %
Fever	12	75 %
Dyspnea	6	37,5 %
Renal failure	6	37,5 %
Laboratory results		
Interleukin-6 (IL6)	5774,72 ng/l	159,00 - 35.152,00 ng/l
C-reactive protein (CRP)	216,36 mg/l	36,00 - 512,00 mg/l
Ferritin	18.037,71 µg/l	1.025,00 - 228.225,00 µg/l
Procalcitonin (PCT)	1.996,92 µg/l	0,47 - 5.300,00 µg/l
Lactate dehydrogenase (LDH)	870,42 U/l	256,00 - 5.267,00 U/l
Troponin T (cTnT)	54,65 ng/l	2,07 - 126,00 ng/l
Treatment		
Hydroxychloroquine	10	62,5 %
Lopinavir/Ritonavir	5	31,25 %
Antibiotics	12	75 %

ACTEMRA (Tocilizumab)	5	31,25 %

Listed laboratory results correspond to the highest (LDH, cTnT), latest (IL6, ferritin, PCT) or last value before administration of ACTEMRA/Tocilizumab (CRP).

Extended Data Table 1b. Clinical Data, Control cohort (6 patients)

Characteristics	N or x	% or range
Postmortem interval	31,4 h	25 - 46 h
Age	81,3 y	63 - 104 y
Sex	M 5 : F 1	

Extended Data Table 1c. Clinical Data, Cohort of patients with other infections (4 patients)

Characteristics	N or x	% or range
Postmortem interval	31,5 h	12 - 79 h
Age	79,5 y	58 - 81 y
Sex	M 2 : F 2	

Patients were suffering from other infections of the lung (bacterial or viral pneumonia). Detailed analysis of individual pathogens is shown in Extended Data Figure 1.

Extended Data Table 2. OIRRA gene list

ABCF1	CCL5	CD40LG	CTAG2	FASLG	HIF1A	IFIT1	IL3RA
ADGRE5	CCNB2	CD44	CTLA4	FCER1G	HLA-A	IFIT2	IL4
ADORA2A	CCR1	CD47	CTSS	FCGR1A	HLA-B	IFIT3	IL6
AIF1	CCR2	CD48	CX3CL1	FCGR2B	HLA-C	IFITM1	IL7
AKT1	CCR4	CD52	CX3CR1	FCGR3A	HLA-DMA	IFITM2	IL7R
ALOX15B	CCR5	CD53	CX3CR1	FCGR3B	HLA-DMB	IFNA17	IRF1
ARG1	CCR6	CD6	CX3CR1	FCRLA	HLA-DOA	IFNB1	IRF4
AXL	CCR7	CD63	CX3CR1	FOXM1	HLA-DOB	IFNG	IRF9
B3GAT1	CD14	CD68	CXCL1	FOXO1	HLA-DPA1	IGF1R	IRS1
BAGE	CD160	CD69	CXCL10	FOXP3	HLA-DPB1	IGSF6	ISG15
BATF	CD163	CD70	CXCL11	FUT4	HLA-DQA1	IKZF1	ISG20
BCL2	CD19	CD74	CXCL13	FYB	HLA-DQA2	IKZF2	ITGA1
BCL2L11	CD1C	CD79A	CXCL8	G6PD	HLA-DQB2	IKZF3	ITGAE
BCL6	CD1D	CD79B	CXCL9	GADD45GIP1	HLA-DRA	IKZF4	ITGAL
BRCA1	CD2	CD80	CXCR2	GAGE1	HLA-DRB1	IL10	ITGAM
BRCA2	CD209	CD83	CXCR3	GAGE10	HLA-E	IL10RA	ITGAX
BST2	CD22	CD86	CXCR4	GAGE12J	HLA-F	IL12A	ITGB1
BTLA	CD226	CD8A	CXCR5	GAGE13	HLA-F-AS1	IL12B	ITGB2
BUB1	CD244	CD8B	CXCR6	GAGE2C	HLA-G	IL13	ITGB7
C10orf54	CD247	CDK1	CYBB	GATA3	HMBS	IL15	ITK
C1QA	CD27	CDKN2A	DDX58	GBP1	ICAM1	IL17A	JAML
C1QB	CD274	CDKN3	DGAT2	GNLY	ICOS	IL17F	JCHAIN
CA4	CD276	CEACAM1	DMBT1	GPR18	ICOSLG	IL18	KIAA0101
CBLB	CD28	CEACAM8	EBI3	GRAP2	ID2	IL1A	KIR2DL1
CCL17	CD33	CIITA	EFNA4	GUSB	ID3	IL1B	KIR2DL2
CCL18	CD37	CLEC4C	EGFR	GZMA	IDO1	IL2	KIR2DL3
CCL2	CD38	CMKLR1	EGR2	GZMB	IDO2	IL21	KLF2
CCL20	CD3D	CORO1A	EGR3	GZMH	IFI27	IL22	KLRB1
CCL21	CD3E	CRTAM	EIF2AK2	GZMK	IFI35	IL23A	KLRD1
CCL22	CD3G	CSF1R	ENTPD1	HAVCR2	IFI44L	IL2RA	KLRF1
CCL3	CD4	CSF2RB	EOMES	HERC6	IFI6	IL2RB	KLRG1
CCL4	CD40	CTAG1B	FAS	HGF	IFIH1	IL2RG	KLRK1

KREMEN1	MLANA	POLR2A	SSX2	TNFSF9
KRT5	MMP2	POU2AF1	STAT1	TOP2A
KRT7	MMP9	PRDM1	STAT3	TP63
LAG3	MPO	PRF1	STAT4	TRIM29
LAMP1	MRC1	PSMB9	STAT5A	TUBB
LAMP3	MS4A1	PTEN	STAT6	TWIST1
LAPTM5	MTOR	PTGS2	TAGAP	TYROBP
LCK	MX1	PTK7	TAP1	VCAM1
LCN2	MYC	PTPN11	TARP	VEGFA
LEXM	NCAM1	PTPN6	TBP	VTCN1
LILRB1	NCF1	PTPN7	TBX21	XAGE1B
LILRB2	NCR1	PTPRC	TCF7	ZAP70
LMNA	NCR3	PTPRCAP	TDO2	ZBTB46
LRG1	NECTIN2	PVR	TFRC	ZEB1
LRP1	NFATC1	PYGL	TGFB1	
LST1	NFKBIA	RB1	TIGIT	
LY9	NKG7	RORC	TLR3	
LYZ	NOS2	RPS6	TLR7	
M6PR	NOTCH3	S100A8	TLR8	
MAD2L1	NRP1	S100A9	TLR9	
MADCAM1	NT5E	SAMHD1	TNF	
MAGEA1	NTN3	SDHA	TNFAIP8	
MAGEA10	OAS1	SELL	TNFRSF14	
MAGEA12	OAS2	SH2D1A	TNFRSF17	
MAGEA3	OAS3	SH2D1B	TNFRSF18	
MAGEA4	PDCD1	SIT1	TNFRSF4	
MAGEC2	PDCD1LG2	SKAP2	TNFRSF9	
MAPK1	PECAM1	SLAMF7	TNFSF10	
MAPK14	PGF	SLAMF8	TNFSF13B	
MELK	PIK3CA	SNAI1	TNFSF14	
MIF	PIK3CD	SNAI2	TNFSF18	
MKI67	PMEL	SRGN	TNFSF4	

Extended Data Table 3. Differentially expressed genes, COVID-19 versus controls

ID	logFC	logCPM	PValue	FDR
DMBT1_64696575	5.086440047	9.507465672	8.27E-12	3.29E-09
TDO2_55162	3.60666041	9.53520997	3.39E-11	6.12E-09
IFI6_47156	3.778639284	14.24783272	4.61E-11	6.12E-09
KIAA0101_319426	3.146999681	8.549063739	8.30E-11	8.26E-09
IGF1R_12291338	-1.346908853	10.50777116	1.63E-10	1.29E-08
MELK_300401	2.899390615	7.833266318	9.68E-10	6.29E-08
BUB1_701803	2.429206201	8.360010662	1.11E-09	6.29E-08
ISG15_66173	4.276622596	13.15626013	1.97E-09	9.78E-08
IFI27_37143	1.911305772	12.5471898	3.00E-09	1.33E-07
PSMB9_384491	1.385731366	10.9106894	6.49E-09	2.58E-07
OAS3_667776	2.754666249	9.890613941	9.75E-09	3.53E-07
CDK1_837939	2.262910126	9.211945164	1.08E-08	3.59E-07
HLA-G_483585	4.030812546	6.375748944	1.47E-08	4.35E-07
SLAMF8_9071016	2.293400189	9.725983998	1.53E-08	4.35E-07
MLANA_159265	-5.75771358	0.738276085	1.83E-08	4.86E-07
CDKN3_434534	1.939803243	8.894315977	2.32E-08	5.46E-07
OAS1_757865	2.607400402	11.38534225	2.33E-08	5.46E-07
JAML_78188	-1.759772394	7.103911839	6.73E-08	1.49E-06
IRS1_37283828	-1.354465089	10.24560172	7.98E-08	1.62E-06
OAS2_15981707	2.021713176	10.70108718	8.12E-08	1.62E-06
CXCL11_261361	4.712702755	12.17691208	8.78E-08	1.66E-06
IDO1_268369	2.77746775	10.21297062	1.32E-07	2.38E-06
FOXM1_10551166	3.511025369	7.302016812	3.85E-07	6.66E-06
LAMP3_12361344	2.218476016	9.184121563	4.93E-07	8.17E-06
IFIT3_72174	2.826535538	12.01665835	6.87E-07	1.07E-05
MAD2L1_115221	1.749064486	8.034765012	7.01E-07	1.07E-05
CD38_519628	1.940842458	9.824900589	7.36E-07	1.08E-05

CCR1_54149	1.473037432	10.11920316	8.34E-07	1.19E-05
GZMB_581688	1.898001877	10.41173908	8.96E-07	1.23E-05
LAG3_13111419	2.386185632	7.994487875	1.01E-06	1.34E-05
TCF7_677799	-1.154491364	6.98289475	1.15E-06	1.48E-05
IFI44L_12771376	2.551619364	11.04872147	1.20E-06	1.49E-05
TOP2A_27522855	2.412862908	9.724530736	1.28E-06	1.55E-05
KLF2_9111017	-1.146655278	10.32922348	1.82E-06	2.13E-05
MX1_232336	2.598359407	11.58716187	2.53E-06	2.88E-05
CXCL9_149250	2.475393657	11.64602422	3.36E-06	3.71E-05
CD276_12011310	1.404468545	6.909158714	3.83E-06	4.12E-05
STAT1_18871996	1.341291438	12.54396256	4.11E-06	4.31E-05
IFI35_419526	1.590766479	9.999010988	4.93E-06	5.03E-05
IFIH1_20172123	1.978276916	9.64184768	5.53E-06	5.50E-05
CCL18_198296	2.559340347	11.50058854	6.63E-06	6.43E-05
KLRB1_177284	-1.356445562	10.32648685	7.21E-06	6.84E-05
CXCR4_100208	-1.262015044	12.69186025	8.67E-06	8.03E-05
GBP1_771872	1.624043959	12.95069926	1.21E-05	0.000109887
CEACAM8_745847	-2.38182276	6.835412175	1.51E-05	0.000133479
IFIT2_124224	2.601872644	12.64896588	1.80E-05	0.000155644
PDCD1LG2_315423	1.435337704	9.765019917	1.94E-05	0.000164473
CXCL10_354459	2.921361689	12.20854003	2.10E-05	0.000173779
IFIT1_158259	3.138880653	12.7962216	2.30E-05	0.000186992
BCL6_21502257	-1.128692675	11.38395943	2.37E-05	0.000188627
CD69_195303	-1.167440855	10.29551815	2.49E-05	0.000194401
PTGS2_14761583	-1.787690656	9.487046641	3.11E-05	0.000229188
CD226_9021006	-1.055303117	8.204262834	3.51E-05	0.000249595
C1QB_111199	1.318021235	14.14106331	5.40E-05	0.000370819
CXCL13_202307	2.634779914	10.17220128	5.53E-05	0.000372978

CCNB2_9861095	2.451586323	8.610014511	6.34E-05	0.000420281
BRCA2_98179922	1.408177984	6.624940626	6.59E-05	0.000429787
MKI67_581686	1.830582251	9.016084457	8.31E-05	0.000533209
BCL2_10401144	-1.054459851	7.084554684	9.27E-05	0.000576492
DDX58_540643	1.637092216	11.5957064	0.000122508	0.000750128
KLRG1_410518	-1.049817337	6.871878081	0.000129441	0.000780569
SNAI2_722828	1.272531289	9.779931728	0.000139876	0.000830906
POU2AF1_230337	1.981866553	9.738343726	0.000172607	0.000967573
XAGE1B_469547	2.99835029	4.93494266	0.000177305	0.000980102
C1QA_67171	1.197339812	12.61310409	0.000183576	0.000989574
PTPRC_710817	-1.011649066	9.527123762	0.000183991	0.000989574
CCL17_288394	-1.834523807	6.992710035	0.0002361	0.001220359
CD1C_12531357	-2.519073627	6.111702351	0.000306038	0.001541811
MPO_15121620	-1.908031327	8.211592408	0.00032134	0.001598665
CCR5_85193	1.040859769	9.653446555	0.00037676	0.001851239
CD83_480580	-1.053864486	8.523628945	0.000393979	0.001889203
CRTAM_312417	-1.623243078	5.490123515	0.000404446	0.001916303
HERC6_17021806	1.846150693	8.504611085	0.000412365	0.001930837
BST2_218322	1.11377782	14.61484839	0.000474995	0.002148274
HLA-DQB2_142243	-2.208546554	2.6772892	0.000635872	0.00275705
CMKLR1_36143	3.089416269	4.095184302	0.000921508	0.003860634
ISG20_642750	1.288727823	10.51232195	0.001035118	0.004203845
TNFSF18_128228	2.048786407	5.115450907	0.001219778	0.004854718
CD163_21422245	1.190748679	13.00811752	0.001277279	0.005033238
CYBB_14221529	1.034200312	11.76129988	0.001416071	0.005525454
IFITM1_359459	1.094499983	14.73592207	0.001527366	0.005845111
RORC_12011307	-1.232621407	6.368975553	0.001648956	0.00625033
TNFRSF9_894998	-1.557976838	6.277732459	0.002060615	0.007593748

IL2_366451	-1.787299469	2.137968085	0.002118414	0.007735127
IRF4_786895	1.2991475	7.589669323	0.002433884	0.008497246
IL21_368450	2.713025334	3.179107785	0.002892483	0.009924208
FCGR1A_547652	1.358837352	8.984718333	0.003056301	0.010396649
SLAMF7_9161020	1.178583741	10.97955754	0.00366687	0.012263986
GZMA_165265	1.05539306	10.51173829	0.004314939	0.014311214
CCR6_271363	-1.108756703	5.421780719	0.004727498	0.015422493
ARG1_174278	-2.016630732	7.856291723	0.005246505	0.016976497
IL10_491598	1.240451265	6.779053894	0.005949936	0.018944598
TNFRSF17_254359	1.607351136	7.694337923	0.006172838	0.019498329
MAGEC2_249358	-2.203350303	-1.572033969	0.007805425	0.024081854
CXCR5_153252	-1.570791614	3.754056017	0.009131323	0.027955897
KRT5_10631165	2.093456369	10.18852794	0.009780171	0.029488696
KRT7_440543	1.017265847	12.56930876	0.012411449	0.035795337
GAGE10_137250	-2.028791387	1.82618068	0.018144659	0.049462838

Extended Data Table 4. Antibodies and staining conditions

Antibody	Supplier	Product Number	Clone	Dilution	Pretreatment	Staining platform	Detection system
CD3	Novocastra	NCL-L-CD3-565	LN10	1:100	H2(20)100	Bond III	Bond Polymer Refine Red Detection (DS9390)
CD4	Novocastra	CD4-368-L-CE	4B12	1:80	30min ER2 95°C	Bond III	Bond Polymer Refine Red Detection (DS9390)
CD8	Novocastra	NCL-L-CD8-4B11	4B11	1:40	H2(30)95	Bond III	Bond Polymer Refine Red Detection (DS9390)
CD15	Cellmarque	115M	MMA	1:25	H1(20)100	Bond III	Bond Polymer Refine Red Detection (DS9390)
CD20	Agilent	M0755	L26	1:600	H2(20)95	Bond III	Bond Polymer Refine Red Detection (DS9390)
CD68	Agilent	M0876	PG-M1	1:100	E1(5)	Bond III	Bond Polymer Refine Red Detection (DS9390)
CD123	Novocastra	CD123-L-CE	BR4MS	1:20	20min ER2 95°C	Bond III	Bond Polymer Refine Red Detection (DS9390)
CD163	Novocastra	NCL-L-CD163	10D6	1:200	H1(20)100	Bond III	Bond Polymer Refine Red Detection (DS9390)
C3d	Dako	A0063	polyclonal	1:700	E1(10)	Bond III	Bond Polymer Refine Red Detection (DS9390)
C5b-9	Lifespan Biosciences		aE11	1:50	Enzyme 1 (5)	Benchmark GX	OptiView DAB (Bestellnummer: 760-700)
Ki67	Agilent	M7240	MIB-1	1:50	H2(20)95	Bond III	Bond Polymer Refine Red Detection (DS9390)
MPO	Agilent	A0398	polyclonal	1:8000	H2(20)95	Bond III	Bond Polymer Refine Red Detection (DS9390)
p53	Agilent	M7001	D07	1:1200	H1(20)100	Bond III	Bond Polymer Refine Red Detection (DS9390)
PD1	Roche Ventana	760-4895	NAT105	no dilution	CC1 40min	Benchmark GX	OptiView DAB (Bestellnummer: 760-700)
SARS-CoV-2	BioConcept	200-401-A50	Anti-SARS-CoV Nucleocapsid	1:6400	H2(20)95	Bond III	Bond Polymer Refine Red Detection (DS9390)

Extended Data Table 5. Histopathology

Case No.	Severity of histological changes in lungs [1]	DAD stage [2]	Intraalveolar edema [3]	Intraalveolar hemorrhage [3]	Neutrophils [4]	SARS-COV-2 genomes / 10^6 RNaseP copies	SARS-CoV-2 IHC [4]
C12	1	-	1	1	1	673	1
	2	1	1	1	2	2'871	2
	2	1	1	1	2	116'310	3
C13	3	1 and 2	1	1	2	38	0
	3	1 and 2	1	1	2	310	0
	3	1 and 2	1	1	2	225	0
C16	1	1	1	0	1	91	0
	1	1 and 2	1	0	1	20	0
C17	1	2	1	1	1	12	0
	2	1 and 2	1	1	2	25	0
C19	1	1	1	1	1	7'603	2
	1	1	0	1	1	18'867	2
C20	3	1 and 2	1	1	2	145	0
	2	1 and 2	1	1	2	3'205	1
	3	1 and 2	1	1	2	32	0
C21	3	2	0	0	2	119	0
	3	2	0	0	1	53	0
	2	2	0	0	1	119	0
C15	2	1	1	0	2	91'186	3
	2	1	1	0	1	2'993	2
C1	1	-	1	0	1	0.4	0
	1	-	1	0	1	0.0	0
	1	-	1	0	1	0.2	0
C3	2	-	0	0	3	14'311	n.d.
	2	-	1	1	3	249'937	3
	2	-	0	0	3	157'042	2
C4	1	-	0	1	1	314'728	3
	2	-	1	1	1	245'331	3
	2	1	1	1	1	187'540	3
C5	2	-	0	0	1	8	0
	2	1 and 2	0	0	1	180	0
	2	1 and 2	0	1	2	82	0
C6	1	-	0	0	1	10'451	1

	1	-	0	0	1	118'620	3
	1	-	1	0	1	114'407	3
C7	1	1 and 2	0	0	1	12'939	3
	1	1 and 2	0	0	1	1'443	1
	1	1 and 2	0	1	2	16'534	2
C8	1	-	0	0	1	17'598	n.d.
	3	-	1	0	3	316	n.d.
	1	-	0	0	1	139	n.d.
C9	1	-	0	0	1	64'242	n.d.
	1	-	0	0	1	85'137	n.d.
	1	-	1	0	1	29'487	n.d.

At least two different tissue blocks from different areas of the lungs were evaluated for each case.
[1] 1 = slight to moderate changes; 2 = moderate changes; 3 = severe changes
[2] 1 = exudative; 2 = proliferating/organizing; 3 = fibrotic
[3] 1 = yes; 0 = no
[4] 1 = very few or few; 2 = moderate; 3 = numerous

Figure 1

a

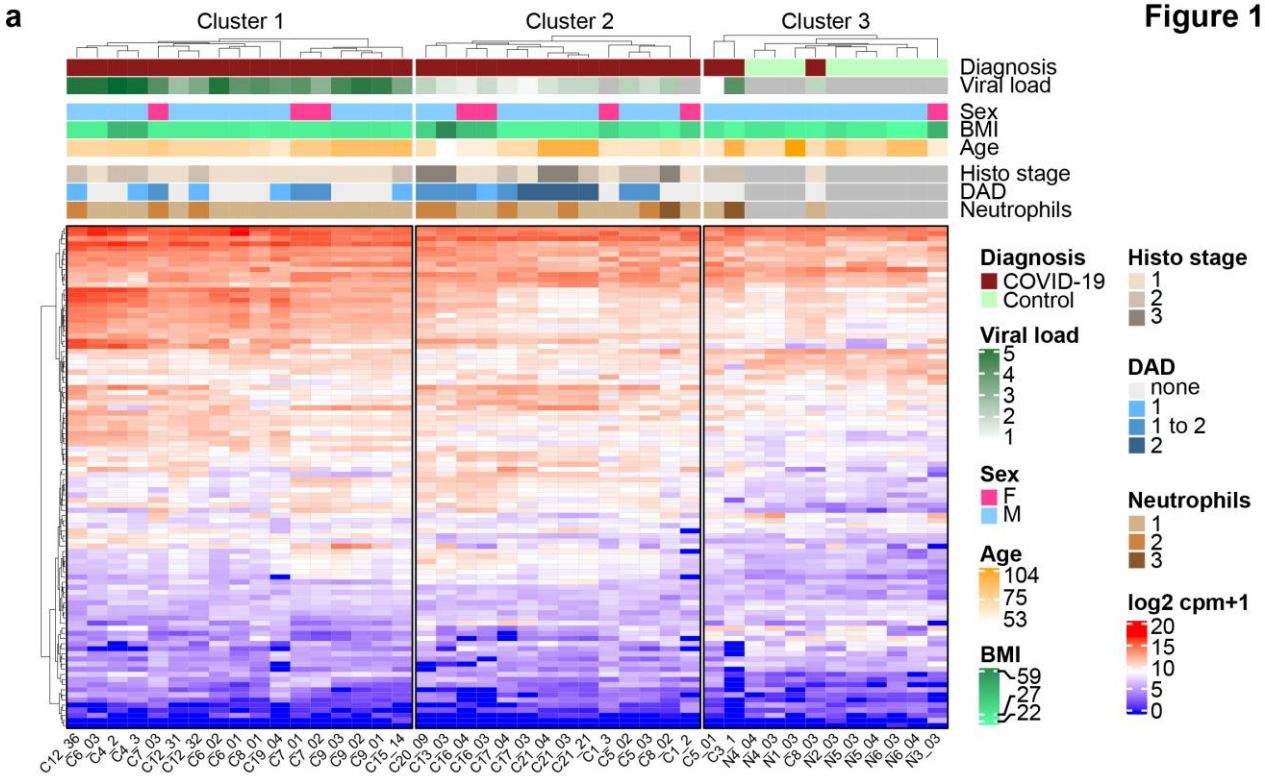

b

ID	Description	GeneRatio	BgRatio	pvalue	p.adjust
GO:0034340	response to type I interferon	17/66	30/379	3.70E-07	0.000158
GO:0060337	type I interferon signaling pathway	17/66	30/379	3.70E-07	0.000158
GO:0071357	cellular response to type I interferon	17/66	30/379	3.70E-07	0.000158
GO:0051607	defense response to virus	21/66	44/379	5.53E-07	0.000177
GO:0098542	defense response to other organism	25/66	71/379	3.85E-05	0.009888
GO:0009615	response to virus	21/66	57/379	9.79E-05	0.020960
GO:0045069	regulation of viral genome replication	10/66	18/379	1.87E-04	0.034381
GO:1903900	regulation of viral life cycle	11/66	22/379	2.95E-04	0.042931
GO:0045071	negative regulation of viral genome replication	8/66	13/379	3.57E-04	0.042931
GO:1903901	negative regulation of viral life cycle	8/66	13/379	3.57E-04	0.042931
GO:0048525	negative regulation of viral process	9/66	16/379	3.68E-04	0.042931
GO:0051603	proteolysis involved in cellular protein catabolic process	7/66	11/379	6.71E-04	0.071789
GO:0050792	regulation of viral process	12/66	28/379	9.17E-04	0.088399
GO:0019079	viral genome replication	10/66	21/379	9.64E-04	0.088399
GO:0043901	negative regulation of multi-organism process	9/66	18/379	1.16E-03	0.099123

c

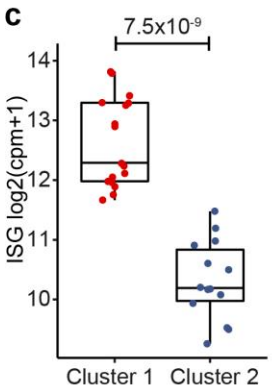

d

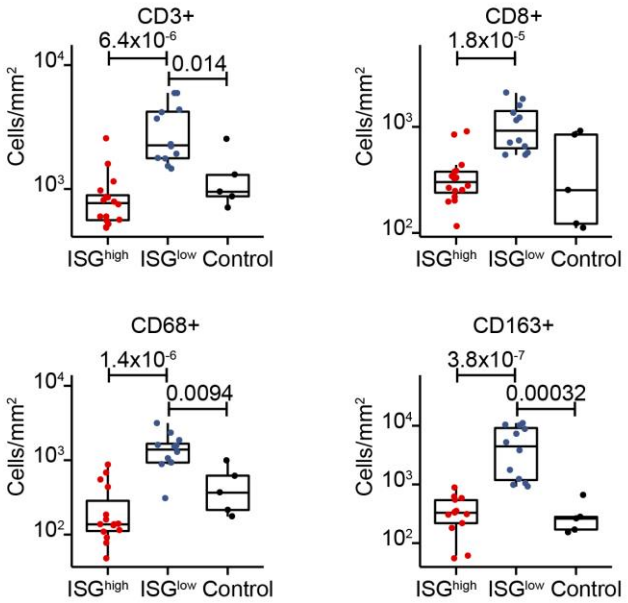

e

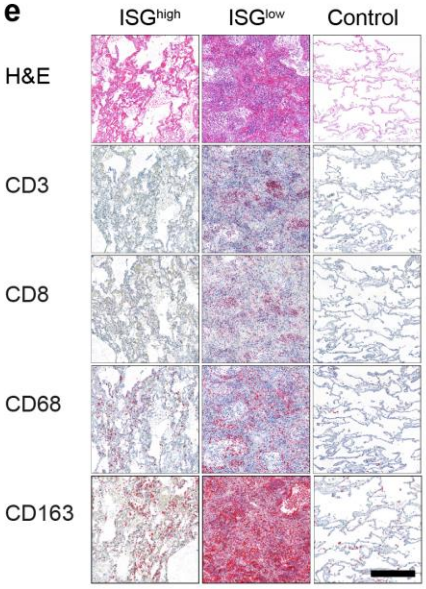

Figure 2

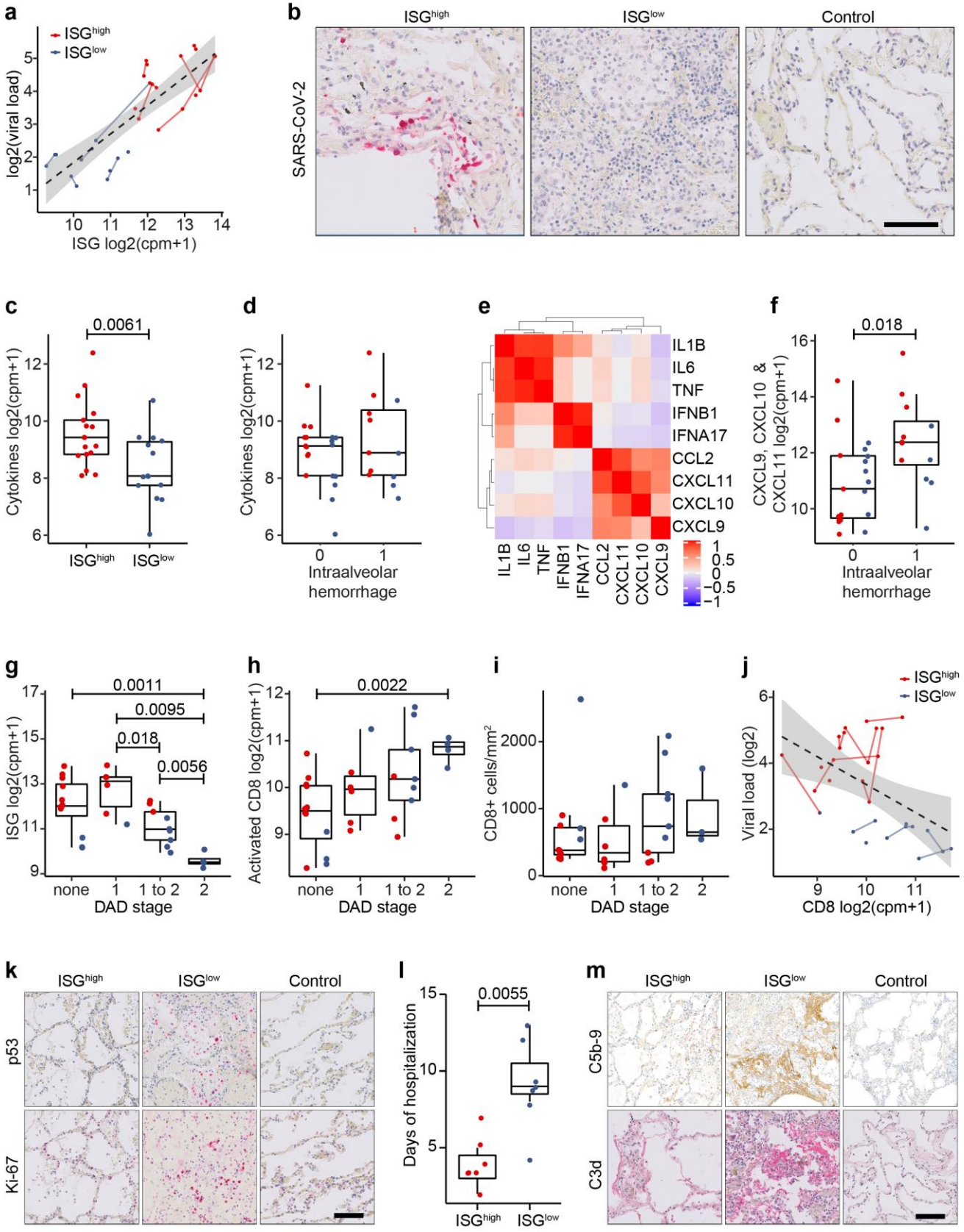
a
ISGhigh
ISGlow
log2(viral load)
ISG log2(cpm+1)
b
ISGhigh
ISGlow
Control
SARS-CoV-2
c
0.0061
Cytokines log2(cpm+1)
ISGhigh
ISGlow
d
Cytokines log2(cpm+1)
Intraalveolar hemorrhage
e
IL1B
IL6
TNF
IFNB1
IFNA17
CCL2
CXCL11
CXCL10
CXCL9
f
0.018
CXCL9, CXCL10 & CXCL11 log2(cpm+1)
Intraalveolar hemorrhage
g
0.0011
0.0095
0.018
0.0056
ISG log2(cpm+1)
none
1
1 to 2
2
DAD stage
h
0.0022
Activated CD8 log2(cpm+1)
DAD stage
i
CD8+ cells/mm²
DAD stage
j
ISGhigh
ISGlow
Viral load (log2)
CD8 log2(cpm+1)
k
ISGhigh
ISGlow
Control
p53
Ki-67
l
0.0055
Days of hospitalization
ISGhigh
ISGlow
m
ISGhigh
ISGlow
Control
C5b-9
C3d

Extended Data Figure 1

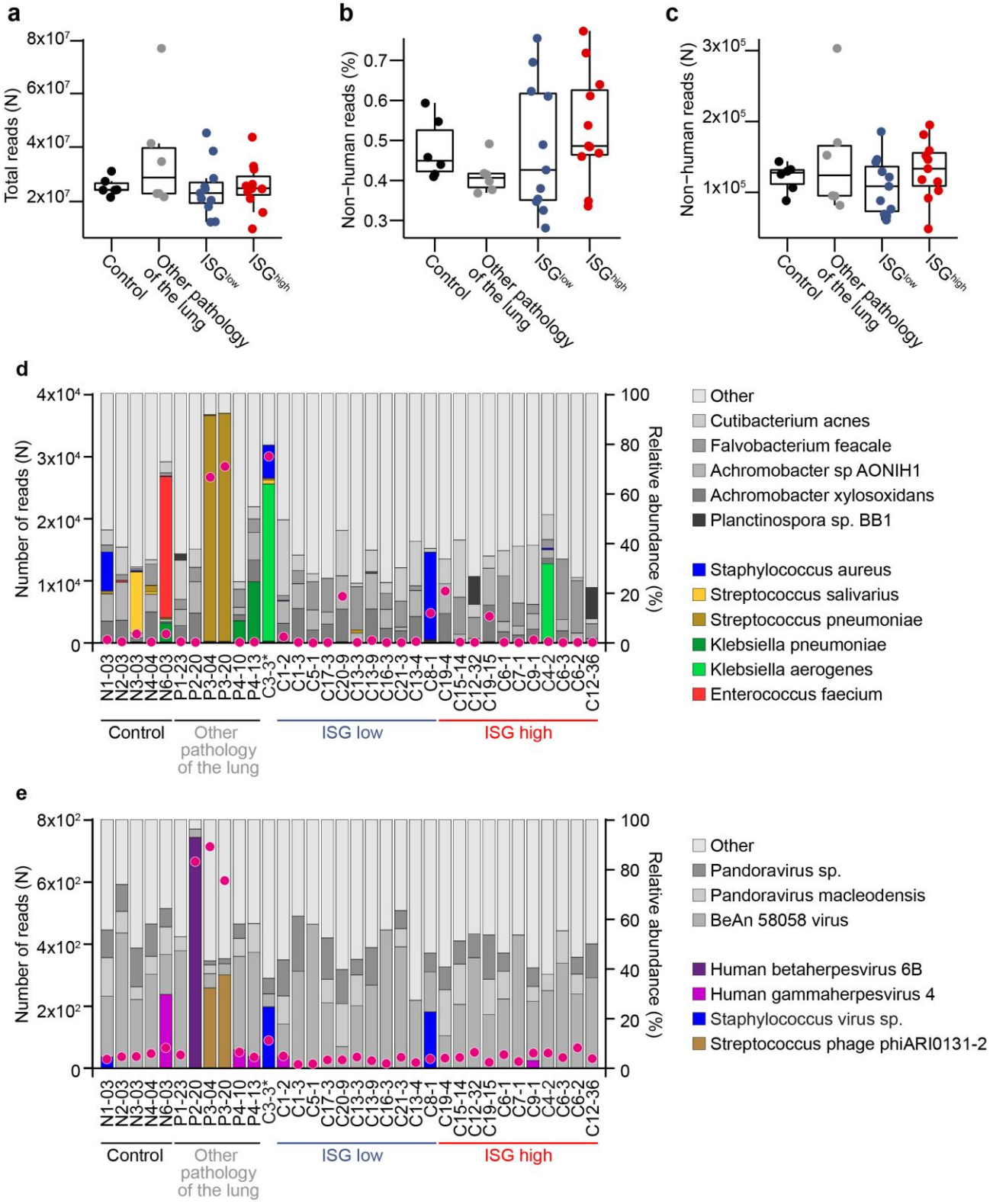

Extended Data Figure 2

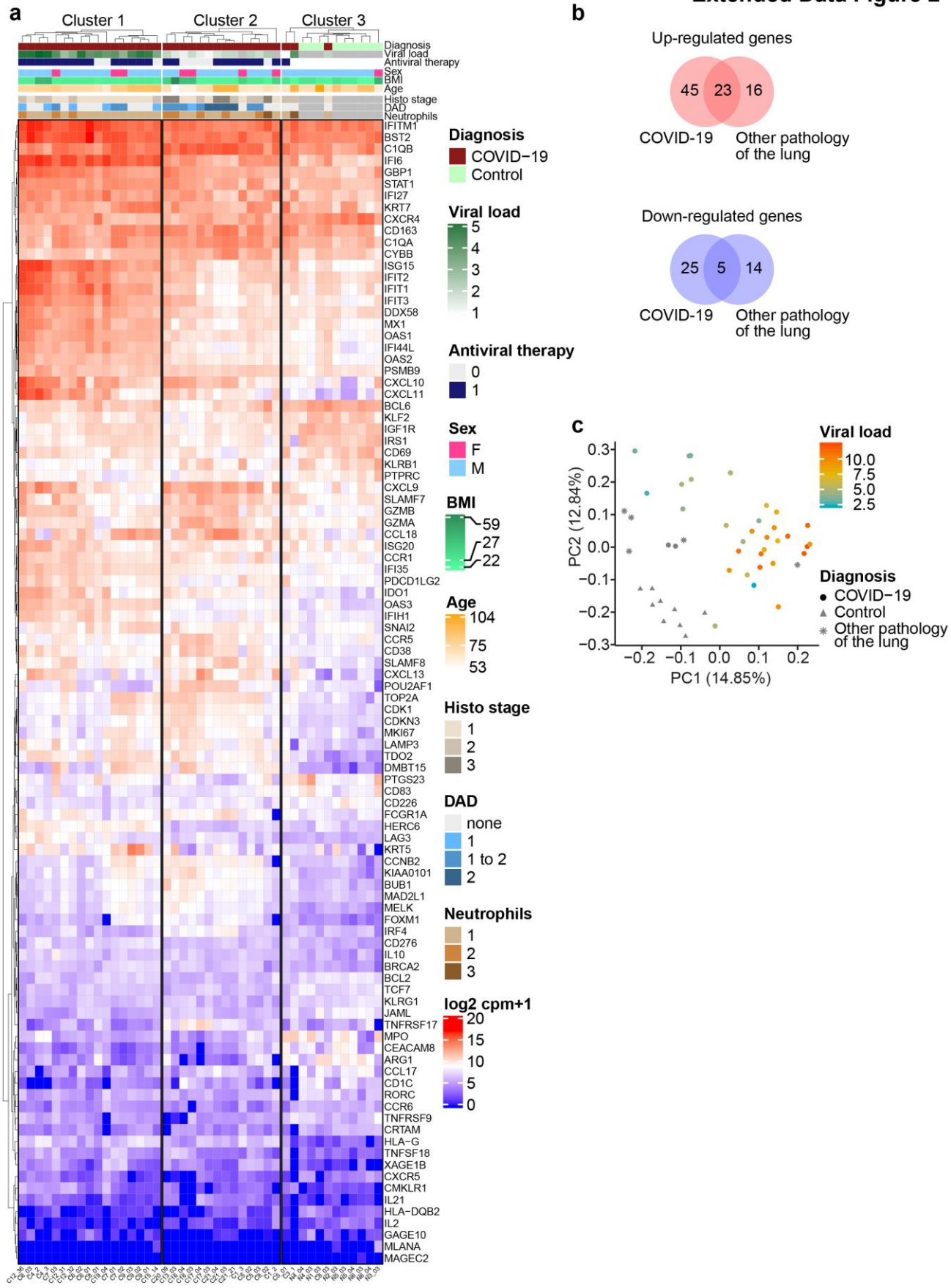

Extended Data Figure 3

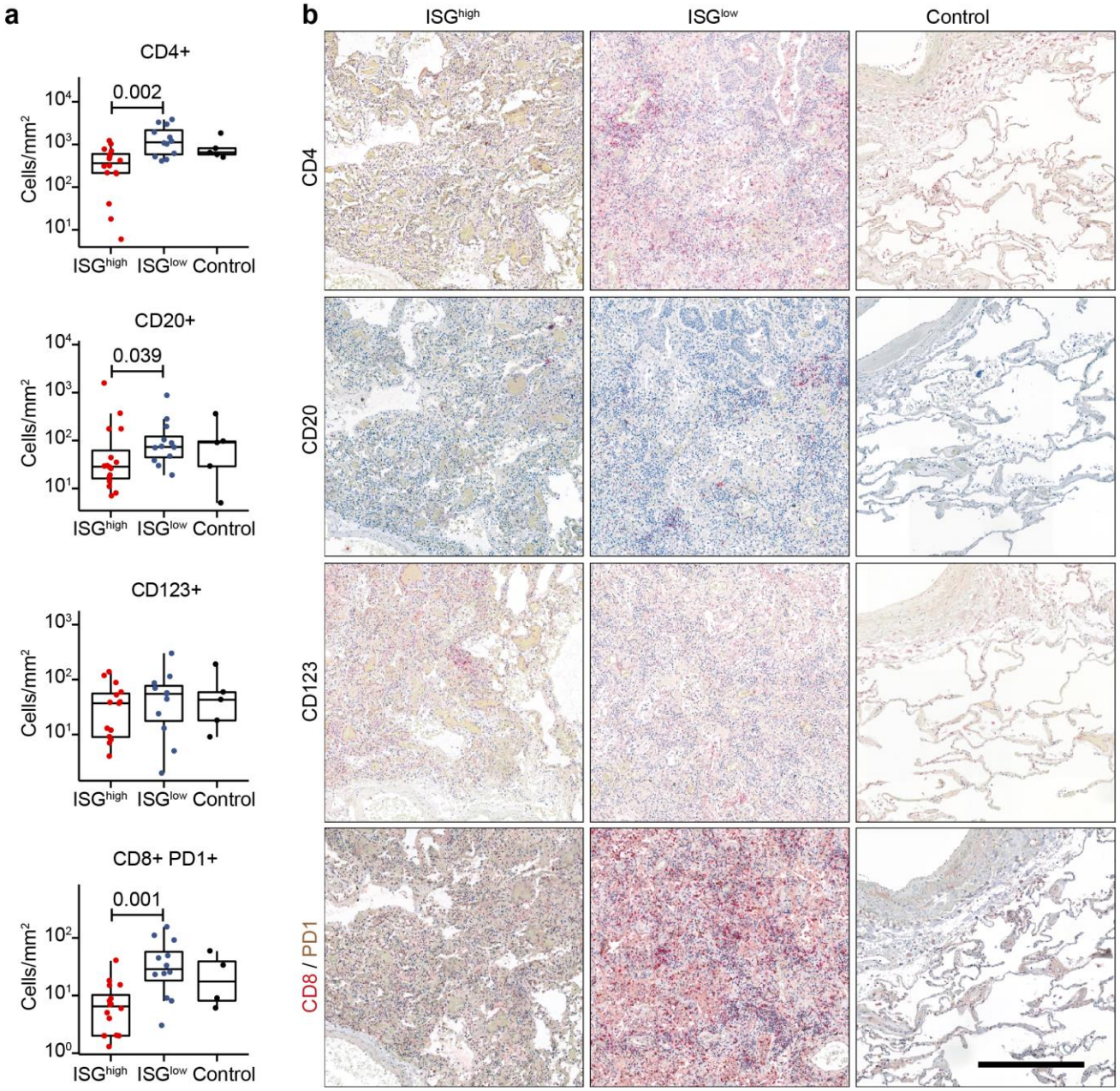

Extended Data Figure 4

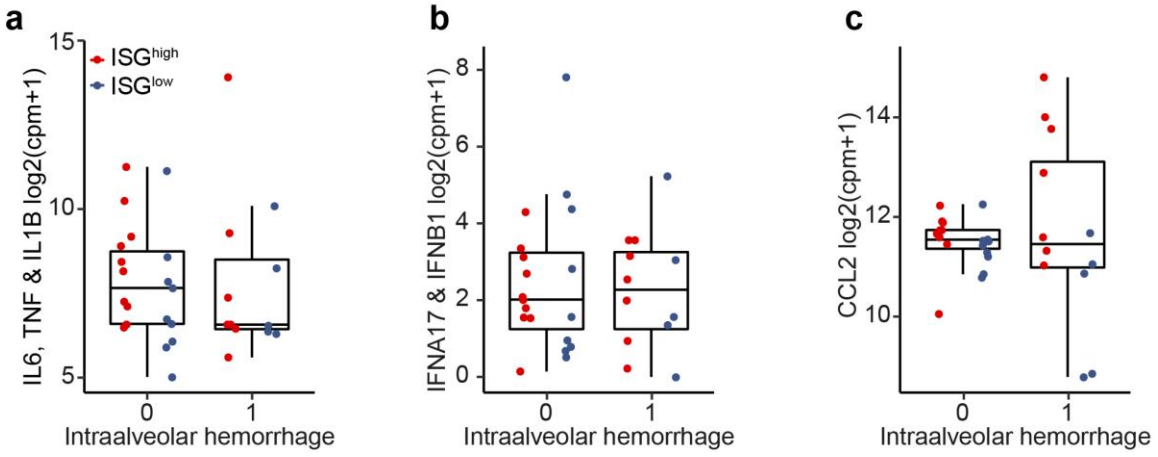
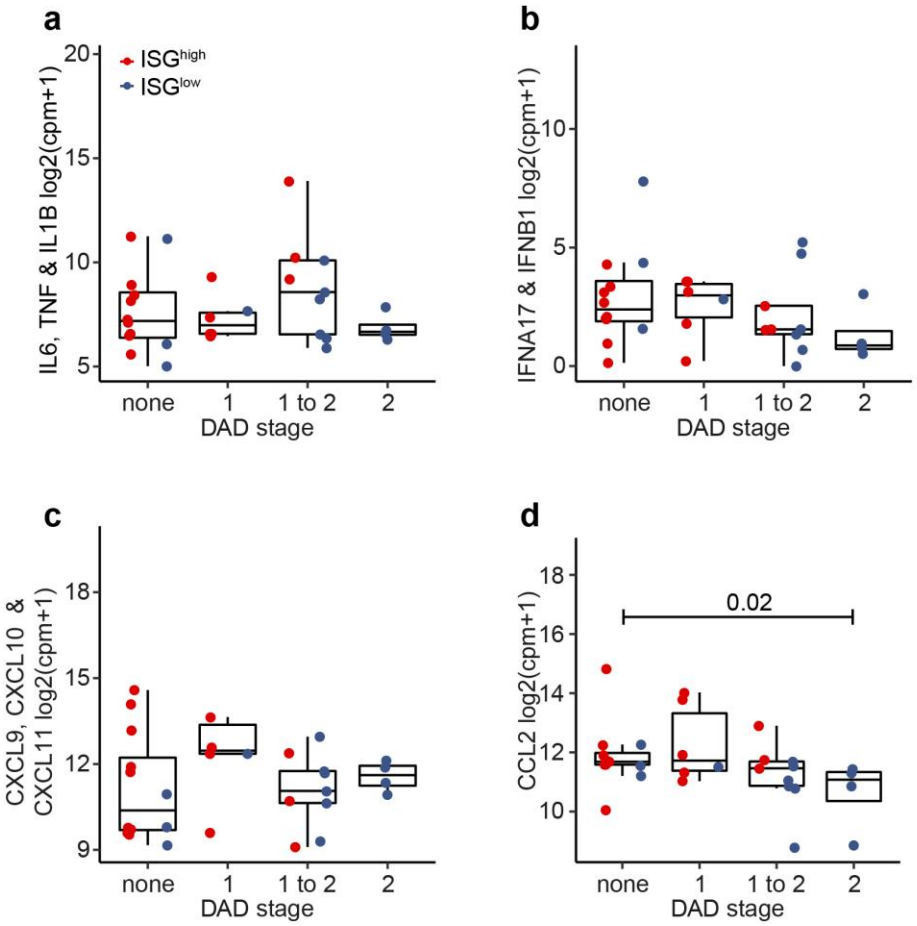
Extended Data Figure 5